

# Spanning the Gap from Bulk to Bin: A Novel Spectral Microphysics Method

E. K. de Jong<sup>1\*</sup>, T. Bischoff<sup>1</sup>, A. Nadim<sup>2</sup>, T. Schneider<sup>1,3</sup>

<sup>1</sup>California Institute of Technology, Pasadena, CA, USA

<sup>2</sup>Institute of Mathematical Sciences, Claremont Graduate University, Claremont, CA, USA

<sup>3</sup>Jet Propulsion Laboratory, California Institute of Technology, Pasadena, CA, USA

## Key Points:

- A new microphysics method using collocation of basis functions is presented.
- The method improves spectral accuracy and precipitation predictions over bulk and bin methods.
- The method applies to a flexible range of computational complexity, providing a way to unify microphysics models.

---

\*

Corresponding author: Emily de Jong, [edejong@caltech.edu](mailto:edejong@caltech.edu)

13 **Abstract**

14 Microphysics methods for climate models typically track one, two, or three moments of  
 15 a droplet size distribution for various categories of liquid, ice, and aerosol. Such meth-  
 16 ods rely on conversion parameters between these categories, which introduces uncertainty  
 17 into predictions. While higher-resolution options such as bin and Lagrangian schemes  
 18 exist, they require too many degrees of freedom for climate modeling applications and  
 19 introduce numerical challenges. Here we introduce a flexible spectral microphysics method  
 20 based on collocation of basis functions. This method generalizes to a linear bulk scheme  
 21 at low resolution and a smoothed bin scheme at high resolution. Tested in an idealized  
 22 box setting, the method improves spectral accuracy for droplet collision-coalescence and  
 23 improves precipitation predictions relative to bulk methods; furthermore, it generalizes  
 24 well to multimodal distributions with less complexity than a bin method. The poten-  
 25 tial to extend this collocation representation to multiple hydrometeor classes suggests  
 26 a path forward to unify liquid, ice, and aerosol microphysics in a single, flexible, com-  
 27 putational framework for climate modeling.

28 **Plain Language Summary**

29 Clouds and aerosols affect global warming by reflecting and absorbing radiation and  
 30 by storing and transporting water. Climate models need a way to efficiently track the  
 31 size and number of cloud droplets, ice, and aerosols in order to accurately predict the  
 32 impact that these “microphysical” particles have on climate. Existing methods of mi-  
 33 crophysics rely on many uncertain parameters and are either too complicated or too sim-  
 34 ple to take advantage of today’s computational resources. We propose a new way to rep-  
 35 resent cloud droplets that can both reduce uncertainties and make use of increased com-  
 36 puting power.

37 **1 Introduction**

38 Droplets, aerosols, and ice particles, collectively a subset of atmospheric microphys-  
 39 ical particles, affect planetary-scale climate, yet the processes that govern their behav-  
 40 ior occur at the microscale. This extreme range of scales, from droplets to clouds to at-  
 41 mospheric dynamics, makes it challenging to computationally represent microphysics.  
 42 There are simply too many particles to represent directly, yet the microphysics processes  
 43 involved are highly nonlinear and do not lend themselves easily to simplifications. In-  
 44 stead, microphysics schemes in climate and numerical weather models predict the par-  
 45 ticle size distribution (PSD) present at various locations in the atmosphere: the PSD and  
 46 number concentration determine the macroscopic behavior of the system, such as cloud  
 47 albedo or precipitation rates. Historically, methods to represent the PSD developed along  
 48 two trajectories: bulk methods, which predict aggregate properties of the droplet pop-  
 49 ulation, and spectral methods, which explicitly track the PSD. Both of these represen-  
 50 tations make assumptions about the droplet distribution and the microphysical process  
 51 rates, with spectral methods being the more flexible of the two options. Unfortunately,  
 52 these parameterizations and assumptions contribute a major yet difficult-to-quantify source  
 53 of uncertainty in climate predictions (Intergovernmental Panel on Climate Change, 2014;  
 54 Morrison et al., 2020; Randall et al., 2003; Khain et al., 2015; Arakawa, 2004).

55 Bulk schemes, originating with Kessler (1969), explicitly track one or more prog-  
 56 nostic moments of the PSD and therefore are very compact representations suitable for  
 57 global climate applications. However, by abstracting a droplet population to one, two,  
 58 or three variables, bulk methods make two fundamental simplifications. First, many single-  
 59 droplet processes such as sedimentation or aerosol activation require parameterizations  
 60 to approximate how the process impacts the prognostic moments. Second, because many  
 61 such process rates depend on higher-order moments which are not explicitly tracked, moment-  
 62 based methods require a closure to relate these higher order moments back to the prog-

63 nostic variables. Frequently this closure is accomplished by relating the prognostic mo-  
64 ments back to an underlying assumed size distribution such as a gamma or exponential  
65 (e.g., Morrison & Grabowski, 2008; Seifert & Beheng, 2006; Milbrandt & Yau, 2005), which  
66 corresponds well to data in many empirical settings. However, in the case of a multimodal  
67 distribution, for instance, when both small cloud droplets and larger rain droplets are  
68 present, this closure assumption introduces significant structural uncertainty into the mi-  
69 crophysics scheme. There is no physical reason, a priori, to restrict a droplet population  
70 to maintaining a particular size distribution as they coalesce, break up, grow, sediment,  
71 and change phases. Unfortunately, inverting a multimodal distribution analytically is  
72 frequently ill-posed (Morrison et al., 2019). Most traditional bulk methods avoid the is-  
73 sue by representing several categories of hydrometeors (rain, cloud droplets, and several  
74 categories of aerosols) through separate prognostic moments, assuming a simple unimodal  
75 distribution for each of these categories. However, these categories of condensed water,  
76 while intuitive, are artificial: in reality, liquid hydrometeors are distributed across a con-  
77 tinuous spectrum, from small chemically-active aerosol particles, to large liquid cloud  
78 droplets, to droplets which are large enough to fall as rain. Conversion between these  
79 categories adds further complexity and uncertainty to the model.

80 On the other hand, spectral or “bin” microphysics schemes directly evolve the PSD  
81 in time through discrete bins, or particle size ranges (e.g., Tzivion (Tzitzvashvili) et al.,  
82 1987; Berry, 1967; Berry & Reinhardt, 1974; Young, 1974). Bin methods have made a  
83 great impact in understanding aerosol-cloud interactions (e.g., Morrison & Grabowski,  
84 2007; Khain et al., 2015), but at a higher computational cost that currently makes them  
85 infeasible for climate simulations. For example, Gettelman et al. (2021) ran a general  
86 circulation model (GCM) with bin microphysics, incurring a factor of five cost penalty  
87 over a bulk scheme. Furthermore, while bin methods avoid the closure assumptions of  
88 bulk schemes, they suffer from numerical challenges (Morrison et al., 2019) as well as from  
89 sensitivity to the bin discretization (Ghan et al., 2011). The purpose of the method pre-  
90 sented here is to target the middle ground of complexity, between traditional bulk and  
91 bin methods, using more sophisticated numerical techniques.

92 To meet the needs of future climate and weather models, a microphysics scheme  
93 should maintain enough flexibility to function with a wide range of degrees of freedom  
94 and minimal structural uncertainty in the PSD representation. While bin-scheme com-  
95 plexity may be unattainable for GCMs in the near future, we still need a microphysics  
96 method that can maintain spectral details without the closure assumptions and conver-  
97 sion parameterizations required by moment-based bulk methods. Some recent efforts in  
98 microphysics modeling have focused on relaxing assumptions about the size distribution  
99 and process rates to reduce these structural uncertainties. One option, Lagrangian mi-  
100 crophysics, directly tracks tracer particles known as superdroplets (Riechelmann et al.,  
101 2012; Andrejczuk et al., 2010, 2008; Shima et al., 2009), but it is far too computationally  
102 expensive for global or even regional models. A different moment-based method, the  
103 BOSS scheme proposed by Morrison et al. (2019) leaves all process rates and closures  
104 as generalized power series whose parameters are learned from data. Bieli et al. (n.d.)  
105 present a more efficient way to learn these parameters within a similar bulk microphysics  
106 framework that still relies on closures. More complex yet, Rodríguez Genó and Alfonso  
107 (2022) tackle the challenge of inverting multimodal distribution closures using a machine-  
108 learning based method, which could avoid the necessity for cloud-rain conversion rate  
109 parameterizations. However, these bulk methods cannot function in a wide range of com-  
110 putational degrees of freedom, nor do they provide complete spectral details about the  
111 PSD that might alleviate uncertainties about conversion between hydrometeor types. One  
112 solution is to think beyond the classical bulk versus bin representations of the PSD, lever-  
113 aging numerical techniques developed for fluid mechanics.

114 In this study, we present and test a novel way to span the gap in complexity be-  
115 tween bin and bulk microphysics methods by applying the collocation method with ba-

116 sis functions (BFs) to represent the particle size distribution. (For simplicity, it will be  
 117 referred to going forward as the BF method.) Finite element methods such as collocation  
 118 have been historically overlooked for microphysics applications, with the exception  
 119 of Gelbard and Seinfeld (1978)’s demonstration using collocation of quartic or cubic poly-  
 120 nomials, which was never widely adopted in favor of contemporaneous bin methods. More  
 121 recent results from the applied math community suggest that combining collocation with  
 122 radial basis functions, rather than polynomials, is a promising numerical technique for  
 123 advection problems (Zhang et al., 2000; Franke & Schaback, 1998). This work extends  
 124 the basis function collocation technique to the integro-differential equations encountered  
 125 in microphysics. Beyond retaining spectral details of the PSD, the BF method has ap-  
 126 pealing extremes of complexity: at low resolutions, the method is effectively a linear clo-  
 127 sure, as in the context of bulk schemes; at moderate or high resolutions, it converges to-  
 128 ward a smoothed bin scheme (replicating a bin scheme exactly if constant piecewise BFs  
 129 and appropriate numerics are used). Therefore collocation of basis functions promises  
 130 greater flexibility than either bulk or bin methods alone, while retaining desirable aspects  
 131 such as low-to-moderate complexity and spectral predictions. This paper describes the  
 132 method and presents results of applying the method to droplet collision and coalescence,  
 133 benchmarked against commonly used bulk, bin, and Lagrangian frameworks. We addi-  
 134 tionally address some limitations posed by the method that are specific to the context  
 135 of tracking a PSD, such as mass non-conservation and a finite size range. Overall, the  
 136 BF method improves spectral PSD predictions in a box model as well as simple precip-  
 137 itation predictions, measured as a size exceedance, compared to a three-moment bulk  
 138 method, and with fewer degrees of freedom than a bin method. Furthermore, the run-  
 139 time complexity of the method scales quadratically with the number of degrees of free-  
 140 dom, making it just as efficient as or faster than a bin method.

141 The remainder of this paper is organized as follows: section 2 describes the method  
 142 of collocation of basis functions to approximately solve the population balance equation  
 143 for collision-coalescence in microphysics, and section 3 describes a set of microphysics  
 144 box model case studies. Section 4 compares the accuracy of these case studies solved us-  
 145 ing basis functions, bulk, bin, and Lagrangian schemes, and discusses the computational  
 146 complexity of these methods. Finally, section 5 concludes the paper and suggests poten-  
 147 tial improvements and applications.

## 148 2 Method Description

### 149 2.1 Key Equations

The governing equations for microphysics describe a population balance for the droplet  
 size distribution. The governing equation for collision-coalescence, also called the Smolu-  
 chowski or Stochastic Collection Equation (SCE), is given by

$$\partial_t n(x, t) = \frac{1}{2} \int_0^x n(x-y, t)n(y, t)K(x-y, y)E_c(x-y, y)dy - n(x) \int_0^\infty n(y, t)K(x, y)E_c(x, y)dy, \quad (1)$$

150 where  $n(x, t)$  represents the number density of particles of mass  $x$  at time  $t$ ,  $K(x, y)$  is  
 151 the collision rate of particles of masses  $x$  and  $y$ , and  $E_c(x, y)$  is the coalescence efficiency  
 152 of said collision. The first integral represents production of droplets of size  $x$  from two  
 153 smaller droplets, and the second integral represents loss of droplets of size  $x$  due to co-  
 154 alescence with other droplets.

Other microphysical processes such as condensation, evaporation, sedimentation,  
 and aerosol activation also affect the PSD. To demonstrate the proposed BF method for  
 microphysics, we initially focus on only the coalescence process as in equation (1). The  
 SCE is notoriously difficult to solve numerically, as it is an integro-partial differential equa-

tion and frequently involves rapid acceleration of particle growth, yet this mechanism is crucial to determining the onset of rain and drizzle (Stephens et al., 2010). Later, we will also consider two non-collisional processes of sedimentation and injection of new particles. Sedimentation is defined as removal all particles above a size threshold  $x_{\max}$ , which can prevent unphysically rapid acceleration of collisions. Sedimentation is enforced by limiting the upper bound of each integral to  $x_{\max}$ , effectively truncating the PSD to have a value of  $n(x > x_{\max}, t) = 0$ . We can alternatively prevent particles larger than the maximum size  $x_{\max}$  from forming by rejecting those collisions in a mass conserving manner. The appropriate upper bound for the second integral in this case is  $x_{\max} - x$  (Filbet & Laurençot, 2004). When such collisions are not rejected and particles exit the system, we introduce new droplets to the system, mimicking entrainment or activation of new particles. The rate of particle injection  $P_{\text{inj}}(x, t)$  is given by

$$P_{\text{inj}}(x, t) = \dot{P}I(x) \tag{2}$$

155 where  $I(x)$  represents a normalized size distribution of the injected droplets, which might  
156 be smaller than the average droplet in the system, and  $\dot{P}$  is the rate of particle injection.

157 **2.2 Collocation of Basis Functions with Positivity Constraint**

In our proposed method, based on the work of Zhang et al. (2000), the PSD is approximated by a weighted sum of  $n_{\text{BF}}$  basis functions:

$$n(x, t) \approx \tilde{n}(x, t) = \sum_{k=1}^{n_{\text{BF}}} c_k(t) \phi(x; \theta_k) = \mathbf{c}(t) \cdot \boldsymbol{\phi}(x). \tag{3}$$

158 We denote the approximate solution  $\tilde{n}(x, t)$ , the collocation weights  $c_k(t)$ , and the ba-  
159 sis functions  $\phi(x|\theta_k)$  where  $\phi$  is the functional form and  $\theta_k$  are the parameters of the  $k$ -  
160 th BF (for instance, mean and variance of a Gaussian). In the collocation method, one  
161 such parameter is the center or mean of the basis function,  $\mu_k \in \theta_k$ , known as the col-  
162 location points. In the context of microphysics, these collocation points refer to parti-  
163 cle masses, which locate the mode of each basis function. In equation (3), we have also  
164 compactly rewritten the BFs and weights in vector form as  $\boldsymbol{\phi}(x) = (\phi(x|\theta_1), \phi(x|\theta_2), \dots, \phi(x|\theta_{n_{\text{BF}}}))$   
165 and  $\mathbf{c}(t) = (c_1(x), c_2(x), \dots, c_{n_{\text{BF}}}(x))$ .

166 Since the basis functions have a fixed shape over the droplet size range, evolving  
167 the approximate PSD reduces to solving for  $\mathbf{c}(t)$  in time as a system of ordinary differ-  
168 ential equations. Because liquid water is a conserved quantity in the absence of evap-  
169 oration/condensation, we consider the evolution of the local mass density  $m(x, t) = x n(x, t)$   
170 rather than the local number density. Thus although we use basis functions to approx-  
171 imate the number density, the equations are evolved in time based on local mass den-  
172 sity, as in a one-moment bulk method or a standard flux-method bin scheme.

Denote the vector of approximate mass density at the collocation points  $\mu_k$  to be  $\tilde{\mathbf{m}}(t) = (\mu_1 \tilde{n}(\mu_1, t), \dots, \mu_p \tilde{n}(\mu_p, t))$ . At each timestep, recovering the weights from the interpolated collocation points requires solving for  $\mathbf{c}(t)$  in the linear system

$$\tilde{\mathbf{m}}(t) = \boldsymbol{\Phi} \cdot \mathbf{c}(t) \tag{4}$$

173 where  $\boldsymbol{\Phi}$  is a  $n_{\text{BF}} \times n_{\text{BF}}$  matrix, with elements  $\Phi_{jk} = \mu_j \phi_k(\mu_j)$  representing the mass  
174 density of the  $k$ -th basis function evaluated at the  $j$ th collocation point. For a linearly  
175 independent set of basis functions, this system is well-posed and guarantees a unique so-  
176 lution. However, it may be ill-conditioned, particularly when the choice of basis func-  
177 tion has global rather than compact support (Zhang et al., 2000).

The approximate solution is initialized by projecting the initial mass distribution onto the basis space. This projection comes from solving an optimization problem:

$$\min_{\mathbf{c}(0)} \|\boldsymbol{\Phi} \cdot \mathbf{c}(0) - \tilde{\mathbf{m}}(0)\|^2 \quad \text{s.t.} \quad \mathbf{c}(0) \geq 0. \tag{5}$$

178 The positivity constraint mathematically enforces the fact that the PSD should be non-  
 179 negative at all points. Equation 5 is formulated as a quadratic optimization, and there-  
 180 fore can be solved efficiently numerically.

181 This projection could additionally incorporate a mass conservation constraint, both  
 182 initially and at every future time step, but at significantly higher cost than solving the  
 183 linear system in equation 4. Additionally, since the exact solution to the equation does  
 184 not necessarily exist as a projection of the basis functions, the mass and positivity con-  
 185 straints in the optimizer can lead to unphysical solutions as the approximate PSD evolves  
 186 in time. While relaxing this constraint might lead to an artificial reduction or increase  
 187 in mass throughout the simulation time, it allows a more efficient nonnegative least-squares  
 188 solution. In developing this method, we observed that evolving the linear system in mass  
 189 density with a positivity constraint, rather than using number density directly, led to  
 190 more physical and realistic PSDs compared to including a mass-conserving constraint  
 191 at all times.

### 192 **2.2.1 Interpretability and design choices**

193 The method described above generalizes to solve many categories of differential equa-  
 194 tion, but selecting the basis functions and parameters  $\theta_k$  requires care in order to pre-  
 195 serve physical properties of a droplet distribution. To model a droplet PSD, we choose  
 196 to let the basis functions themselves be distributions, in contrast to the cubic splines em-  
 197 ployed by Gelbard and Seinfeld (1978) or spectral element methods. If we choose Gaus-  
 198 sian or lognormal BF's collocated on a grid of droplet sizes, each BF effectively repre-  
 199 sents a droplet size mode. This feature provides a useful analogy to aerosol size modes,  
 200 or cloud versus rain droplet distributions, much as a typical bin scheme will distinguish  
 201 between aerosol, cloud, and rain size bins, or how a moment scheme will have a sepa-  
 202 rate set of moments for cloud and rain water. In fact, this representation is a general-  
 203 ization of bin schemes, which can be considered piecewise constant basis functions:  $\phi_k(x) =$   
 204  $1, x \in \{x_k, x_{k+1}\}$  (see figure 1). At low resolution, the BF representation can similarly  
 205 be thought of as approximating a linear closure, as in the method of moments (MOM),  
 206 where the prognostic variable is the first moment calculated over sub-intervals of the par-  
 207 ticle size range.

208 Additional design choices include selecting the collocation points and additional  
 209 hyperparameters of the BFs, such as the variance for lognormal or Gaussian distribu-  
 210 tions. An in-depth description and justification of the BF setup used in following sec-  
 211 tions can be found in Appendix A. Notably, we introduce a compactly-supported BF that  
 212 approximates a lognormal distribution (CSLBF1: equation A1), use exponentially-spaced  
 213 collocation points, and set the geometric standard deviation as the distance between ad-  
 214 jacent collocation points.

### 215 **2.3 Application to the SCE and microphysical processes**

The equations involved in applying the BF method to the SCE are derived in ap-  
 pendix B, with the result summarized by equation 6 below:

$$\begin{cases} d_t \tilde{\mathbf{m}}(t) = \mathbf{c}(t) \cdot \mathbf{Q} \cdot \mathbf{c}(t) + \sum_{l=1}^{N_{proc}} \mathbf{P}_l \\ \Phi \cdot \mathbf{c}(t) = \tilde{\mathbf{m}}, \quad \text{with } \mathbf{c}(t) \geq 0 \end{cases} \quad (6)$$

216 In this equation, third-order tensor  $\mathbf{Q}$  and vectors  $\mathbf{P}_l$  are obtained by taking various in-  
 217 ner products of the collision kernel and additional process rates (respectively) with the  
 218 basis functions. All integrals for this collision-coalescence term can be pre-computed for  
 219 a fixed set of basis functions, defining these tensors through numerical integration and  
 220 projection of rate processes onto the basis space. (The required precomputations and  
 221 scaling of these computations with the number of BFs are described in Appendix B. In  
 222 summary, the precomputation steps scale at most cubically with the number BFs, and

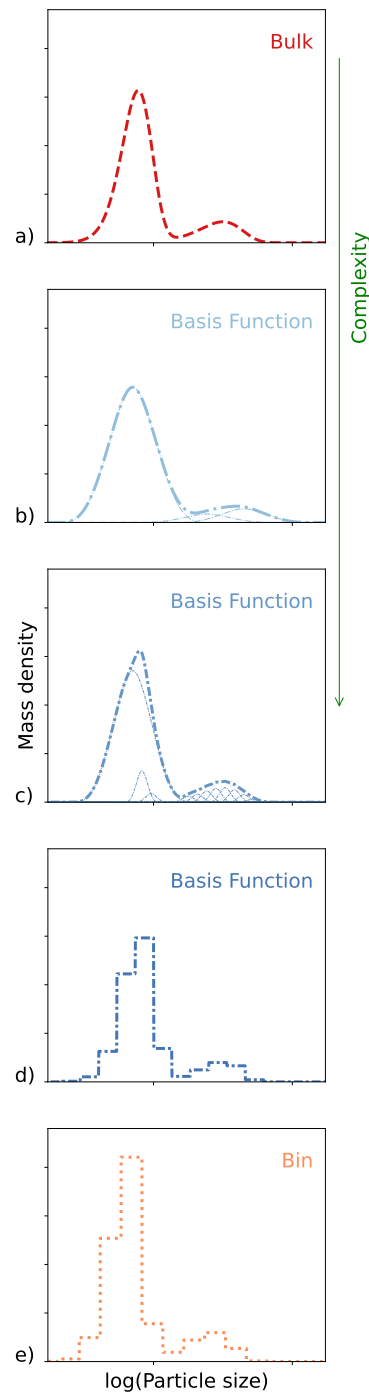


**Figure 1.** Illustration of the way that the collocation of basis functions can span the gap from bulk to bin microphysics. The PSD for a two-mode gamma mixture of particles, corresponding, for instance, to a cloud and rain mode, is plotted as it would be represented in a: (a) 3-moment bulk scheme with gamma closure (one set of moments for each mode); (b) 4 lognormal basis functions; (c) 16 lognormal basis functions; (d) 16 piecewise-constant basis functions; (e) bin method with 32 bins.

Case	Dynamics	Parameters	Duration	Initial/Injection Distribution
1C	Constant kernel	$A = 10^{-4} \text{cm}^3 \text{s}^{-1}$	360s	Gamma $\theta = 100 \mu\text{m}^3$ $N_0 = 100 \text{cm}^{-3}, k = 3$
1G	Golovin kernel	$B = 1500 \text{s}^{-1}$	4hr	
1H	Hydrodynamic kernel	$C = \pi \times 10^{-9} \text{cm}^{-3} \mu\text{m}^{-4} \text{s}^{-1}$	360s	
2	Golovin kernel	$B = 1500 \text{s}^{-1}$	4hr	Gamma mixture $N_{0,a} = 100 \text{cm}^{-3}$ $k_a = 4, \theta_a = 100 \mu\text{m}^3$ $N_{0,b} = 100 \text{cm}^{-3}$ $k_b = 2, \theta_b = 15 \mu\text{m}^3$
3	Golovin kernel, Injection, Precipitation	$B = 1500 \text{s}^{-1}$ $P_{\text{inj}} = 1 \text{cm}^{-3} \text{s}^{-1}$ $x_{\text{max}} = 1000 \mu\text{m}^3$	4hr	Gamma distribution, $\theta = 100 \mu\text{m}^3$ $N_0 = 0, k = 3$

**Table 1.** Summary of the dynamics, parameters, and initial or injection distributions employed for each box model test case.

223 the computation at each time step scales cubically or quadratically depending on the ba-  
 224 sis chosen.) The result is a simple set of quadratic coupled ordinary differential equa-  
 225 tions for the mass density at the collocation points,  $\mathbf{m}(t)$ , and the BF weight vector  $\mathbf{c}(t)$ .

### 226 3 Test Cases

227 To compare the accuracy and efficiency of the proposed BF method with bin, bulk,  
 228 and Lagrangian microphysics schemes, we use three sets of dynamics in a zero-dimensional  
 229 box. The parameters for these experiments are summarized in table 1.

230 The first test case evolves a PSD with collision-coalescence dynamics only, begin-  
 231 ning from a single droplet size mode following a gamma distribution with number den-  
 232 sity  $N_0$ , shape parameter  $k$  and scale parameter  $\theta$ . We consider a constant collection ef-  
 233 ficiency  $E_c = 1$  and three separate collision kernels: (1C) a constant rate of collision  
 234  $K_C(x, y) = A$ ; (1G) a Golovin linear kernel (Golovin, 1963)  $K_G(x, y) = B(x+y)$ , and  
 235 (1H) a hydrodynamic kernel  $K_H(x, y) = C(r(x) + r(y))^2 |a(x) - a(y)|$ , where  $r(x)$  and  
 236  $a(x)$  represent the particle radius and area respectively. Collision kernel parameters and  
 237 time of simulations are chosen such that the final droplet spectrum has approximately  
 238 1/3 the number density of the initial spectrum. We investigate the PSD (mass density)  
 239 following collisions, as well as the first three moments of the PSD which correspond to  
 240 total number density, mass density, and radar reflectivity. Spectral errors are calculated  
 241 as a sum of squared differences in the approximated profiles and a reference solution from  
 242 Lagrangian microphysics. In addition, we calculate the percent mass exceedance over a  
 243 droplet-size threshold of  $x_{\text{max}} = 1000 \mu\text{m}^3$ . This exceedance can be considered a proxy  
 244 for precipitation, even though all mass remains in the box.

245 The second test case retains the Golovin collision kernel but uses a two-mode ini-  
 246 tial distribution: a sum of two gamma distributions. This initial distribution can be thought  
 247 of as representing two aerosol modes, or alternatively a cloud mode and rain droplet mode.  
 248 A simple closure-based bulk representation cannot capture multiple modes without an  
 249 additional set of prognostic moments and autoconversion rates; therefore, this test case  
 250 highlights the information gained from using a more flexible PSD representation.

251 The third test case incorporates additional dynamics of particle injection and pre-  
 252 cipitation from the box. Given a constant prescribed injection rate, this set of dynam-

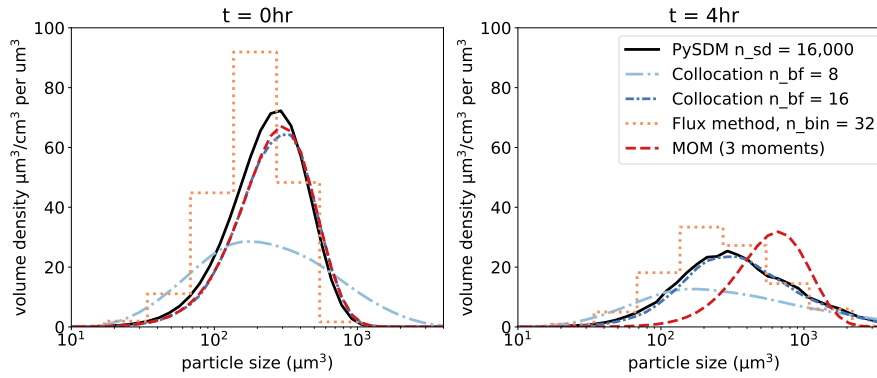


**Figure 2.** Initial spectrum (left) and post-collision spectrum (right) resulting from a Golovin kernel collision-coalescence (1G) for bulk (MOM), bin (flux), and Lagrangian methods, and using the BF (collocation) method with 8 or 16 degrees of freedom.

253 ics will drive the PSD to a steady state in which particles enter the system, collide, grow,  
 254 and precipitate out of the system. While modeling collision-coalescence by itself is a use-  
 255 ful numerical test, it requires that the microphysics scheme be able to represent arbitrar-  
 256 ily large particles with an accelerating rate of growth. Using a simplified proxy for the  
 257 introduction of small droplets and removal of large droplets allows for a more physically  
 258 realistic particle size distribution and time scale of dynamics.

259 We solve each test case numerically using the flux method for spectral bin micro-  
 260 physics with 32 bins (Bott, 1998), a three-moment gamma-closure method of moments  
 261 (Bieli et al., n.d.), and collocation of BFs with varying numbers of basis functions, re-  
 262 ferred to as the degrees of freedom. The bin method used follows the original setup from  
 263 Bott (1998), spanning a range of  $1.06\mu\text{m}^3$  to  $2.28 \times 10^9\mu\text{m}^3$  with mass doubling between  
 264 bins. Additionally we include results from a Lagrangian particle-based code called PySDM  
 265 (v2.5) (Bartman et al., 2022) as a high-resolution reference for the first three cases. The  
 266 PySDM simulations use 16,384 superdroplets to represent the particle population in a  
 267 box of volume  $1\text{m}^3$ .

268 The BF method as demonstrated here uses 8 or 16 CSLBF1 basis functions to span  
 269 a particle size range of  $8\mu\text{m}^3$  to  $125,000\mu\text{m}^3$ , which corresponds to 15 of the 32 bins used  
 270 in the bin approach. Collocation points are logarithmically spaced over this size range.  
 271 Particles are assumed spherical with liquid water density. BF shape parameters  $\theta_k$  are  
 272 chosen such that the basis functions overlap with their nearest neighbors:  $\theta_k = \mu_k -$   
 273  $\mu_{k-2}$  and  $\theta_1 = \theta_2 = \mu_2$ . The method is implemented in the Julia programming lan-  
 274 guage and uses a variable time-step with the DifferentialEquations.jl package (Rackauckas  
 275 & Nie, 2017). The inversion is solved using NonNegLeastSquares.jl v0.4.0 (non-negative  
 276 least squares). Numerical integrals are computed using Cubature.jl v1.5.1.

## 277 4 Results

### 278 4.1 Case 1: Unimodal collision-coalescence

279 For the collision-coalescence only box case, we are interested in the ability of each  
 280 microphysics method to accurately predict: (1) the PSD; (2) the first three moments of  
 281 the distribution; and (3) the number of particles above a particular size threshold. The  
 282 spectra in figure 2 reveal that more than eight basis functions are necessary for this par-  
 283 ticular BF configuration to approximate the initial condition’s primary size mode. From

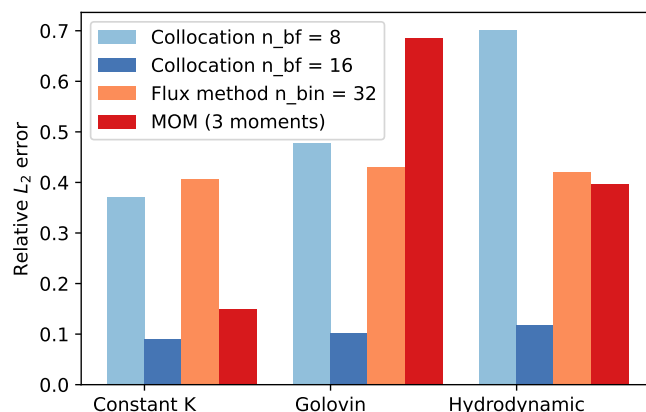


**Figure 3.** Spectral error ( $L_2$ ) for the bulk, bin (flux), and BF methods with 8 or 16 basis functions, computed relative to a Lagrangian PySDM result. Errors are shown for each of three coalescence-only experiments using a constant, Golovin, and hydrodynamic kernel (case 1C, 1G, and 1H, respectively).

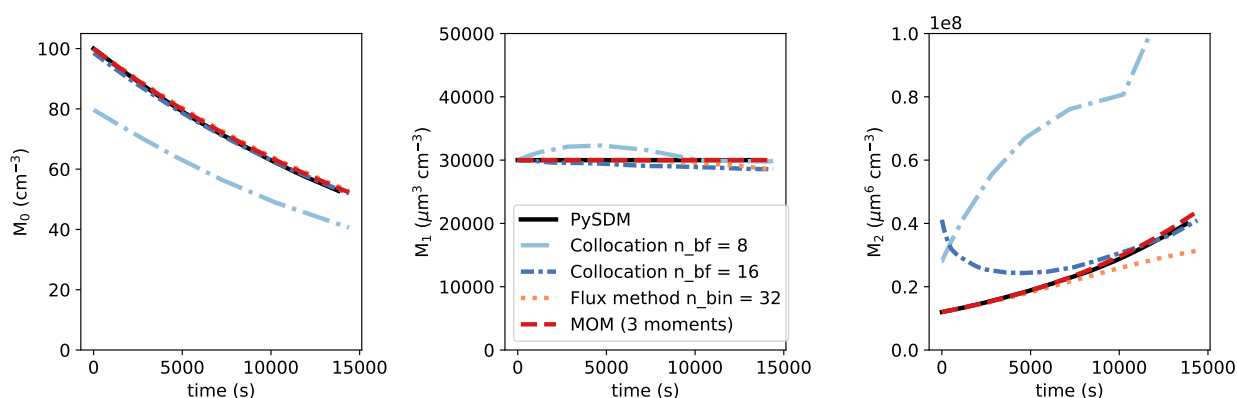


**Figure 4.** Evolution of the first three moments of the PSD over time for bulk, bin, and BF method with 8 or 16 degrees of freedom for the Golovin collision kernel (1G).

284 the final spectra in figure 2 for the Golovin kernel, as well as the summarized spectral  
 285 errors in figure 3, we find that the collocation method with 8 BFs performs on par with  
 286 a flux bin method, and with 16 BFs it outperforms both a bin and bulk method in pre-  
 287 dicting the post-collision spectra. The bin method consistently has a spectral error of  
 288 around 40% relative to the Lagrangian results, owing in part to numerical diffusion, while  
 289 the bulk method of moments has an error which varies significantly according to the com-  
 290 plexity of the collision kernel. While the 8-BF collocation approach suffers from this same  
 291 challenge, using the BF approach with 16 degrees of freedom results in consistently small  
 292 spectral errors less than 15% for all three collision kernels investigated. These results demon-  
 293 strate the potential for the collocation method to resolve realistic droplet spectra using  
 294 the same or fewer degrees of freedom than a traditional bin method.

295 Next we investigate bulk quantities predicted by each method in figures 4 and 5,  
 296 which illustrate the time evolution of the first three moments and exceedance mass, re-

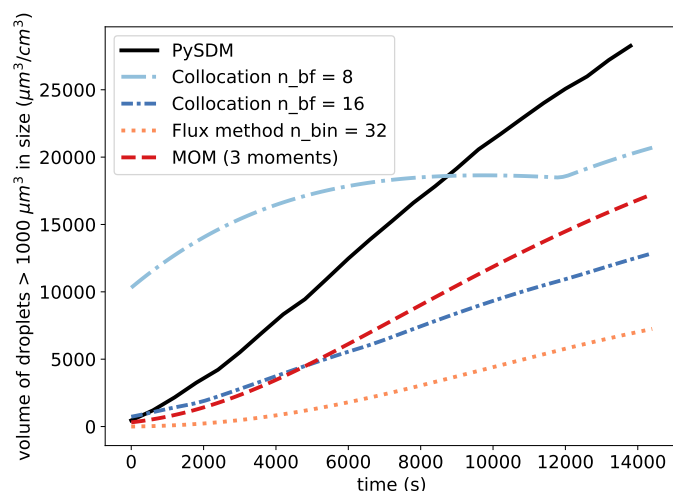


**Figure 5.** Volume of droplets exceeding  $1000\mu\text{m}^3$  in size for Lagrangian, bulk, bin, and collocation methods as a function of time for a Golovin collision kernel (1G).

297 spectively. The bulk method of moments outperforms the BF method in predicting the  
 298 time evolution of the PSD moments, as the first two moments are predicted as prognos-  
 299 tic moments analytically, and the gamma closure approximation is only employed in com-  
 300 puting the second moment. The BF method does not exactly conserve mass in the lower-  
 301 resolution case, in part because the use of compactly supported basis functions prevents  
 302 the representation of particles larger than the support of the basis functions ( $125,000\mu\text{m}^3$   
 303 in this case). Larger particles may form according to the physics of the collision-coalescence  
 304 equation; therefore the BF method encounters error in the tail of the spectral represen-  
 305 tation, and especially in the higher-order moments as a result. Furthermore, the matrix  
 306 inversion in equation 4 does not guarantee conservation of mass, particularly where the  
 307 system of equations might be large and ill-conditioned. The second moment is overes-  
 308 timated by the BF method initially due to error in projecting the initial PSD onto the  
 309 basis space: the initial projection slightly overpredicts the size of some droplets, but not  
 310 so much as to miscategorize them in the exceedance regime larger than  $x_{\text{max}} = 1000\mu\text{m}^3$   
 311 in the higher-resolution BF case, as indicated in figures 2 and 5. Indeed, despite short-  
 312 comings in predicting PSD moments, the BF method does comparably well or better than  
 313 bin or bulk methods at capturing the mass of particles which lie in the tail of the dis-  
 314 tribution (figure 5). It is apparent that the conversion of small particles to medium or  
 315 larger particles is adequately captured by the BF method. All methods underpredict the  
 316 exceedance volume relative to the Lagrangian superdroplet method at longer times, but  
 317 the BF approach displays comparable accuracy to the bulk method of moments and out-  
 318 performs the bin method.

#### 319 4.2 Case 2: Multimodal collision-coalescence

320 One strength of the BF method is its ability to represent up to  $n_{\text{BF}}$  modes of a PSD,  
 321 where  $n_{\text{BF}}$  is the number of basis functions used. By contrast, bulk methods can rep-  
 322 resent at most one droplet mode, and bin methods lose spectral detail of the modes due  
 323 to the piecewise constant representation of the PSD. We demonstrate in figure 6 an ex-  
 324 ample of collision-coalescence with an initially bimodal distribution: the second mode  
 325 initially has a narrower and more peaked structure, which broadens and extends as these  
 326 larger particles collide more rapidly according to the Golovin collision dynamics. The

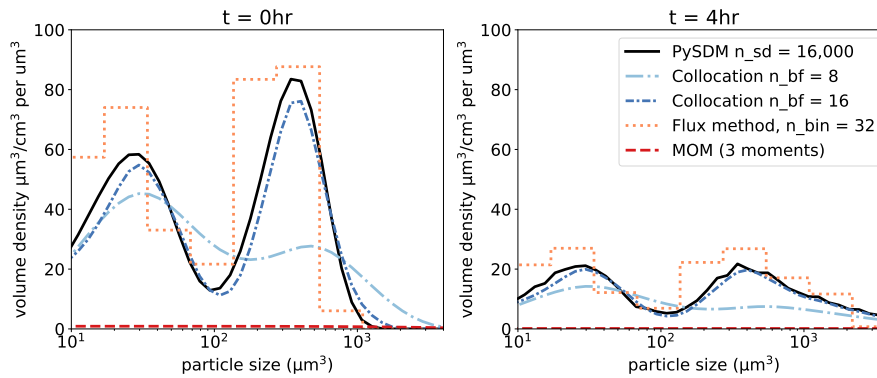


**Figure 6.** Spectra following collision-coalescence of a bimodal droplet population using Lagrangian, bulk, bin, and BF methods with a Golovin kernel (case 2).

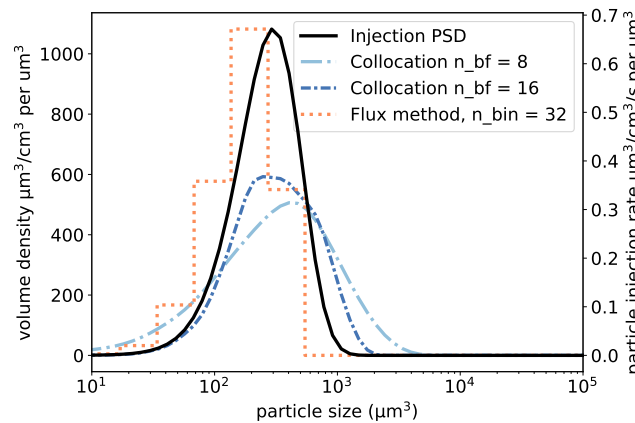


**Figure 7.** Steady state PSD for the third case with collisions, sedimentation, and injection, using a bin method and the BF method with 8 or 16 basis functions. The PSD of injected particles is plotted as a solid black line with units on the right y axis.

327 BF method accurately captures both of these modes during the PSD evolution, while  
 328 the bulk method with a gamma-closure cannot represent the initial or final PSD due to  
 329 the underlying unimodal closure assumption. Furthermore, while the bin method accu-  
 330 rately predicts droplets in both size ranges, the BF method is able to do so with fewer  
 331 degrees of freedom and yields a closer and more interpretable spectral match to the La-  
 332 grangian results.

### 333 4.3 Case 3: Collision-coalescence with injection and removal

334 When including removal of large particles and introduction of small particles, we  
 335 investigate the steady-state PSD as well as the time evolution of the PSD moments. The  
 336 Lagrangian and method of moments simulations are excluded in this case, as the removal  
 337 and injection process rates used are not applicable in these frameworks. As seen in fig-  
 338 ure 7, the BF method solution is a broadened image of the injected PSD, as expected:  
 339 particles enter the system, grow through collisions, and exit once they reach  $1000\mu\text{m}^3$   
 340 in size. As in previous cases, the BF solution is slightly narrower when more degrees of

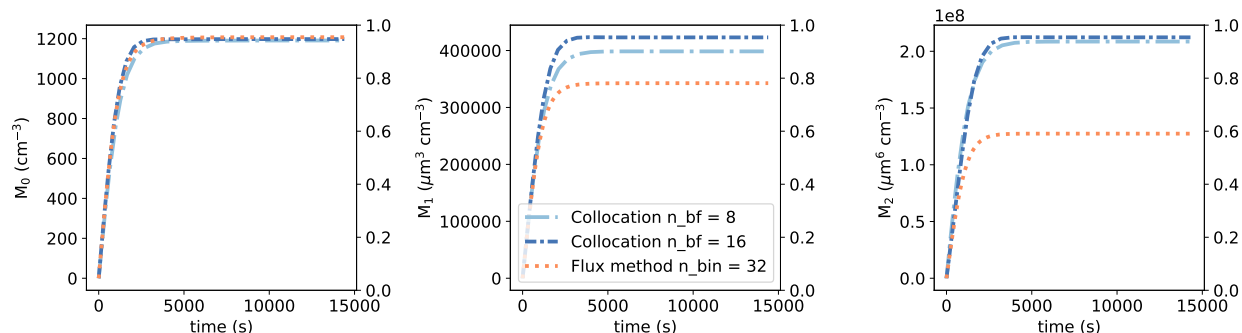


**Figure 8.** Time-series evolution of first three moments of the distribution for the collocation and bin methods with collisions, precipitation, and injection.

341 freedom are used, but the lower-resolution BF case does not display as large of a discrep-  
 342 ancy when large particles are removed. The bin approach underpredicts the steady state  
 343 distribution of larger particles, in part because the piecewise constant representation leads  
 344 to over-removal of particles in the largest bin. This shortcoming is further demonstrated  
 345 in the higher-order moments of the system in figure 8. Both the BF and bin methods  
 346 converge to a steady state on the same time scale, with the same number density, but  
 347 the bin method underpredicts the first and second moments relative to even the lower-  
 348 resolution BF method, demonstrating the improvement possible from using nonlinear  
 349 distributions as a basis, rather than piecewise bins. This more realistic set of dynamics,  
 350 which removes large particles from the system, demonstrates that the BF method using  
 351 collocated compactly supported basis functions is well-suited for representing a complete  
 352 microphysical system at longer GCM-relevant time scales. These results illustrate  
 353 a tradeoff between higher accuracy in the spectrum and moments from using more basis  
 354 functions when coalescence dominates, and the ability to use a lower complexity setup  
 355 with fewer (e.g., 8 versus 16) degrees of freedom when additional compensating dynam-  
 356 ics are considered.

#### 357 4.4 Computational Complexity

358 The BF method offers similar or improved computational scaling relative to the  
 359 bin spectral method, but higher complexity than a traditional multimoment bulk method.  
 360 Bulk methods with a closure assumption scale with the number of moments,  $\mathcal{O}(N_{\text{mom}})$   
 361 when the relationship between the prognostic moments and PSD parameters is known,  
 362 but more complex PSD closures may require nonlinear operations or even optimization,  
 363 leading to a more computationally intensive operation at each time step. Spectral bin  
 364 methods such as the flux method used here (Bott, 1998) scale quadratically with the num-  
 365 ber of bins,  $\mathcal{O}(N_{\text{bin}}^2)$ , as each pair of bins is considered sequentially. The basis function  
 366 method scales either cubically or quadratically depending on the choice of basis (see ap-  
 367 pendix B). While the initial precomputation for the BF method is cubic in the number  
 368 of basis functions, a compactly supported basis will lead to quadratic operations in the  
 369 forward time-marching of equation 6, as the third-order tensor  $\mathbf{Q}$  is sparse. This places  
 370 the BF method at the same order of complexity as other spectral methods,  $\mathcal{O}(N_{\text{BF}}^2)$ .

## 371 5 Discussion and Conclusions

372 This paper describes and demonstrates a novel method to represent the particle  
 373 size distribution of droplets for atmospheric microphysics. Collocation of basis functions

374 provides a more flexible PSD approximation than either bin microphysics or the method  
 375 of moments with closure (bulk microphysics). In particular, selecting BFs which are them-  
 376 selves distributions generalizes traditional spectral bin methods to a smoothed represen-  
 377 tation that can be interpreted as the sum of droplet size modes. The method is also ap-  
 378 propriate for applications where more than three degrees of freedom (the most usually  
 379 provided in a bulk scheme) are desired, but where full bin complexity is infeasible. In  
 380 this low-resolution limit, collocation of basis functions can be considered a form of linear  
 381 closure relating the mass density at the collocation points to a BF weight vector.

382 Tested in a variety of box model settings, we find that the BF method improves  
 383 spectral accuracy under collision-coalescence dynamics compared to a three-moment bulk  
 384 method, while using fewer degrees of freedom than a bin method. The spectral detail  
 385 from the BF approach allows for a more precise calculation of water mass in the tail of  
 386 the distribution (exceedance), which could avert the need for precipitation parameter-  
 387 izations that are required by bulk methods. Another strength of the method is its abil-  
 388 ity to represent multimodal distributions, unlike 3-moment bulk methods. At short time  
 389 scales with rapidly accelerating collisions, the BF method suffers from numerical chal-  
 390 lenges and compact support that cannot represent arbitrarily large particles; therefore,  
 391 we propose an additional set of dynamics that allows removal of large particles from the  
 392 box. In this collision-injection-removal case study, the BF method outperforms a bin scheme  
 393 in computing the steady-state distribution, and it requires fewer degrees of freedom.

394 In general, the BF method is a more flexible framework than bulk or bin methods:  
 395 the suggested implementation can receive an arbitrary set of microphysical processes and  
 396 automatically perform all required numerical integrations. This is in contrast to bin meth-  
 397 ods, which require tabulated collision and breakup kernels that are dependent on the bin  
 398 discretization, and in contrast to bulk methods, which frequently include hard-coded pa-  
 399 rameterizations and closures. This ability to specify arbitrary functional process rates  
 400 for the BF method will be especially useful for reducing microphysics parameter uncer-  
 401 tainty while also improving the structural PSD representation.

402 The BF method does have limitations. First, although the linear system in equa-  
 403 tion 4 is solved in mass density space with a positivity constraint, the method does not  
 404 exactly conserve mass for a collision-coalescence-only set of dynamics. When employed  
 405 with compactly supported basis functions, the method can only represent particles up  
 406 to a maximum size, unlike bulk or Lagrangian methods. This shortcoming manifests in  
 407 errors in the higher order moments of the PSD, including some mass loss from the sys-  
 408 tem (figure 4). Solutions could involve allowing for some globally supported basis func-  
 409 tions, or periodically rescaling the weight vector to exactly conserve mass in the system.  
 410 Nevertheless, despite this limitation, the method is able to predict both spectral details  
 411 and moments when particle removal and injection are considered; therefore, further re-  
 412 finement may be unnecessary to describe a full set of microphysical processes. Future  
 413 work to improve and test this novel microphysics method will involve incorporating ad-  
 414 ditional microphysical processes, as well as employing one, two, and three-dimensional  
 415 simulations to test the ability of the method to reproduce mesoscale cloud properties.  
 416 Further testing of the method in a one-dimensional setting with spatial advection will  
 417 be necessary to assess how susceptible the collocation implementation is to numerical  
 418 diffusion, as is often observed with bin schemes.

419 The BF method presented here improves spectral accuracy at a lower cost per de-  
 420 gree of freedom than bulk or bin methods, and it has the potential to reduce the com-  
 421 putational cost of microphysics even further. Using inspiration from proposed moving  
 422 bin schemes, the locations or shapes of BFs could be periodically updated to maximize  
 423 the information potential provided by only  $n_{\text{BF}}$  degrees of freedom. While this approach  
 424 would impose a higher cost of recomputing numerical integrals, it would cluster basis func-  
 425 tions near the most-weighted droplet modes, improving the accuracy-complexity trade-  
 426 off. Another potential benefit of the collocation representation is the ability to use mul-

427 multidimensional basis functions: one independent variable could be the droplet size, as in  
 428 this work, while other particle properties such as aerosol hygroscopicity, ice riming frac-  
 429 tion, or surface tension could occupy additional inputs. This multidimensional represen-  
 430 tation has been explored for aerosol bin schemes (Lebo & Seinfeld, 2011), as well as for  
 431 ice bulk methods (Morrison & Milbrandt, 2015). However, it may be more computation-  
 432 ally efficient to represent multiple particle properties in the BF framework due to the  
 433 flexibility of selecting basis functions as well as using compact support to generate a sparse  
 434 system and lessen the computational burden. Such a representation could eliminate the  
 435 uncertainties of conversion parameterizations and of information loss from aggregating  
 436 particles into categories with distinct sets of dynamics. This potential provides a path  
 437 toward unifying the numerical representation of all microphysical particles in a single,  
 438 consistent framework.

## 439 **Appendix A Basis functions, collocation points, and hyperparameters**

440 The BF collocation parameters demonstrated in this study are briefly explained.  
 441 As the collocation points correspond to the droplet mode represented by each BF, we  
 442 should not assume a priori any particular initial or final distribution of particles. How-  
 443 ever, we can use the inherent length scales of the physical system to aid the setup. For  
 444 cloud droplets and aerosols, the size domain should extend from  $x_{\min} \geq 0 \mu\text{m}$  to the size  
 445 of the largest particles  $x_{\max}$  that do not sediment out of the system or instantaneously  
 446 break up, hence making a finite domain approximation reasonable. Furthermore, we draw  
 447 inspiration from bin microphysics to suggest logarithmically spaced collocation points  
 448 over the domain.

449 The basis function family and their hyperparameters should then be selected to en-  
 450 sure a few criteria:

- 451 1. The entire domain  $[0, x_{\max}]$  is spanned with some minimum probability.
- 452 2. There should be no particles with negative or infinite mass; that is,  $\phi_k(x < 0), \phi_k(x \rightarrow$   
 453  $\infty) = 0$  for all basis functions.
- 454 3. BF hyperparameters should be selected to minimize oscillations and jumps in the  
 455 approximated distribution.

456 The first condition is equivalent to requiring either globally-supported BFs, such  
 457 that  $\phi(x) > 0 \forall x$ , or sufficient overlap of compactly-supported BFs, which are positive  
 458 over some interval and zero elsewhere. The second condition cannot be met exactly for  
 459 any BFs that are globally supported over  $(-\infty, \infty)$ , therefore we suggest using either compactly-  
 460 supported BFs (CSBFs) or exponentially decaying BFs. CSBFs are additionally recom-  
 461 mended due to their favorable numerical properties: Zhang et al. (2000) demonstrate that  
 462 CSBFs result in a better conditioned system of equations (as in equation 5). The third  
 463 criterion is the trickiest and will depend on the family of BFs chosen. As a simple heuris-  
 464 tic for a two-parameter family such as Gaussians, we suggest setting the scale factors as  
 465 some multiple of the spacing between collocation points to ensure support and smooth-  
 466 ness over the domain. More sophisticated methods of setting the hyperparameters, such  
 467 as optimization over a set of potential distributions or constraints on fluctuations in the  
 468 second derivatives, are possible but beyond the scope of this paper.

469 Several families of basis functions are suitable to approximate a droplet size dis-  
 470 tribution, such as Gaussian, gamma, and lognormal distributions. In order to obtain a  
 471 compactly supported basis, however, we propose to use a version of the CSRBF1, a com-  
 472 pactly supported Gaussian approximation proposed by Wu (1995), modified to instead  
 473 use a logarithmic argument. This basis function, which we will refer to as CSLBF1 (com-  
 474 pactly supported lognormal BF 1) takes the form:

$$\phi(r) = \begin{cases} \frac{12}{35}(1-r)^4(4+16r+12r^2+3r^3)\frac{dr}{dx} & r \leq 1 \\ 0 & r > 1 \end{cases} \quad (\text{A1})$$

with argument

$$r = \frac{|\log(x) - \mu|}{\theta}$$

475 where  $\mu$  is the collocation point and  $\theta$  is a scale factor. Given that CSRBF1 approximates  
 476 a normal distribution, CSLBF1 approximates a lognormal distribution, which is better  
 477 suited to particle distributions as it is right skewed.

## 478 Appendix B Collocation of BFs for the SCE

Evaluating equation 1 with arbitrary additional processes  $\mathbf{P}_1$  in mass density at collocation point  $\mu_j$ , we find:

$$\begin{aligned} \partial_t \mu_j n(\mu_j, t) = & 1/2 \mu_j \int_0^{\mu_j} n(\mu_j - y, t) n(y, t) K(\mu_j - y, y) E(\mu_j - y, y) dy \\ & - \mu_j n(\mu_j, t) \int_0^{x_{\max} - \mu_j} n(y, t) E(\mu_j, y) K(\mu_j, y) dy + \sum_{l=1}^{N_{proc}} P_l(\mu_j, n(\mu_j, t)) \end{aligned} \quad (\text{B1})$$

Substituting the collocation approximate solution for local mass density,  $x\tilde{n}(x, t) = \sum_{k=1}^p x\phi_k(x)c_k(t)$ , this time derivative becomes:

$$\begin{aligned} \partial_t \tilde{m}_j(t) = & 1/2 \sum_{k=1}^{n_{BF}} \sum_{l=1}^{n_{BF}} \mu_j c_k(t) c_l(t) \int_0^{\mu_j} \phi_k(\mu_j - y) \phi_l(y, t) K(\mu_j - y, y) E(\mu_j - y, y) dy \\ & - \sum_{k=1}^{n_{BF}} \sum_{l=1}^{n_{BF}} \mu_j c_k(t) c_l(t) \phi_k(\mu_j) \int_0^{x_{\max} - \mu_j} \phi_l(y) K(\mu_j, y) E(\mu_j, y) dy + \sum_{l=1}^{N_{proc}} \mu_j P_l(\mu_j, \tilde{n}(\mu_j, t)) \end{aligned} \quad (\text{B2})$$

The collision-coalescence dynamics are summarized via a third-order tensor in mass density:  $\mathbf{Q}$ , with

$$Q_{jkl} = 1/2 \mu_j \int_0^{\mu_j} \phi_k(\mu_j - y) \phi_l(y, t) K(\mu_j - y, y) E(\mu_j - y, y) dy - \mu_j \phi_k(x\mu_j) \int_0^{x_{\max} - \mu_j} \phi_l(y) K(\mu_j, y) E(\mu_j, y) dy \quad (\text{B3})$$

479 The overall dynamics are then summarized by cubic collision-coalescence dynamics plus  
 480 the additional processes projected onto the basis space as in equation 5 to obtain the terms  
 481  $\mathbf{P}_l = (\mu_1 P_l(\mu_1), \mu_2 P_l(\mu_2), \dots, \mu_k P_l(\mu_k))$  in equation 6.

482 Many of the quantities in equation 6 can be precomputed and stored for a given  
 483 set of basis functions. These precomputations include:

- 484 • The linear system,  $\Phi$ ;
- 485 • The third order tensor  $\mathbf{Q}$  which can be computed numerically via quadrature or  
 486 Monte Carlo integration, given a functional form of the kernel.
- 487 • Appropriate projection of additional processes onto the basis space to obtain  $\mathbf{P}_l$ .  
 488 For the purpose of ensuring mass conservation, this may require computing the  
 489 first moments of the basis functions over the integration window  $[0, x_{\max}]$ .
- 490 • The initial condition at the collocation points  $\tilde{\mathbf{m}}(0)$ .

491 The computation of  $\mathbf{Q}$  scales cubically with the number of collocation points for  
 492 globally supported basis functions, and quadratically for partially overlapping compactly  
 493 supported basis functions. The dynamical system in equation 6 involves at most cubic

494 vector-tensor multiplication and function evaluations for the tensor-vector inner prod-  
 495 ucts, and therefore a small system of basis functions is more likely to be limited by the  
 496 time-stepping scheme or matrix inversion than by the precomputation. Another advan-  
 497 tage of choosing compactly supported basis functions is that the constant-collocation ma-  
 498 trix  $\Phi$  can be N-diagonal (CSBF's that only overlap their nearest neighbors will result  
 499 in a tridiagonal system, for example) thus making the inversion much more computa-  
 500 tionally efficient. Finally, using CSBFs limits the range of particle sizes to a finite do-  
 501 main, making numerical integration more straightforward.

## 502 Acronyms

503 **BF** Basis function (method)  
 504 **CSBF** Compactly supported basis function  
 505 **CSLBF1** Compactly support lognormal basis function 1  
 506 **GCM** General circulation model  
 507 **MOM** Method of moments  
 508 **PSD** Particle size distribution  
 509 **SCE** Stochastic collection equation

## 510 Notation

511  $x$  Particle mass or volume  
 512  $n(x, t)$  Particle size distribution: number of particles of mass  $x$  in a volume of air at  
 513 time  $t$   
 514  $K(x, y)$  Collision kernel: rate of collisions between particles of mass  $x$  and  $y$   
 515  $E_c(x, y)$  Coalescence efficiency for particles of mass  $x$  and  $y$   
 516  $x_{\max}$  Particle size threshold; particles above this mass are removed from the system  
 517  $P_{\text{inj}}(x, t)$  Injection rate of particles of size  $x$  at time  $t$ , given in number of particles per  
 518 air volume per time  
 519  $\dot{P}$  Injection rate, in number of particles per air volume per time  
 520  $I(x)$  Normalized size distribution of injected particles  
 521  $\tilde{n}(x, t)$  Approximate PSD using a basis function representation  
 522  $c(t)$  Vector of basis function weights at time  $t$   
 523  $\phi(x)$  Vector of basis functions  
 524  $\theta_k$  Hyperparameters of the  $k$ -th basis function  
 525  $\mu_k$  Collocation point of the  $k$ -th basis function  
 526  $\tilde{m}(t)$  Mass density of the  $k$ -th weighted basis function  
 527  $\Phi$  Basis function mass density tensor:  $\Phi_{jk} = \mu_j \phi_k(\mu_j)$   
 528  $Q$  Third order collision kernel tensor in basis function space  
 529  $P_l$  Vector of process rate  $l$  projected onto basis function space

## 530 Acknowledgments

531 We thank Anna Jaruga, Melanie Bieli, Clare Singer, Zach Lebo, and John Seinfeld for  
 532 feedback, insights, and discussion. Additional thanks go to Jakob Shpund for providing  
 533 access to the Bott flux method bin implementation. E. de Jong was supported by a De-  
 534 partment of Energy Computational Sciences Graduate Fellowship. This research was ad-  
 535 ditionally supported by Eric and Wendy Schmidt (by recommendation of Schmidt Fu-  
 536 tures) and the Heising-Simons Foundation. The implementation of basis function col-  
 537 location and examples used in this work can be found in the package RBFCloud.jl at [https://](https://doi.org/10.5281/zenodo.6536677)  
 538 [doi.org/10.5281/zenodo.6536677](https://doi.org/10.5281/zenodo.6536677). The 3-moment bulk scheme uses the package Cloudy.jl,

539 available at <https://github.com/CLiMA/Cloudy.jl>, and the Lagrangian microphysics  
540 package PySDM is available at <https://github.com/atmos-cloud-sim-uj/PySDM>.

541 **References**

- 542 Andrejczuk, M., Grabowski, W. W., Reisner, J., & Gadian, A. (2010). Cloud-  
543 aerosol interactions for boundary layer stratocumulus in the Lagrangian  
544 Cloud Model. *Journal of Geophysical Research: Atmospheres*, *115*(22). doi:  
545 10.1029/2010JD014248
- 546 Andrejczuk, M., Reisner, J. M., Henson, B., Dubey, M. K., & Jeffery, C. A. (2008).  
547 The potential impacts of pollution on a nondrizzling stratus deck: Does aerosol  
548 number matter more than type? *Journal of Geophysical Research: Atmo-*  
549 *spheres*, *113*(19). doi: 10.1029/2007JD009445
- 550 Arakawa, A. (2004). The Cumulus Parameterization Problem: Past, Present, and  
551 Future. *Journal of Climate*, *17*(13), 2493–2525. doi: 10.1175/1520-0442(2004)  
552 017(2493:RATCPP)2.0.CO;2
- 553 Bartman, P., Bulenok, O., Górski, K., Jaruga, A., Łazarski, G., Olesik, M. A., ...  
554 Arabas, S. (2022). PySDM v1: particle-based cloud modeling package for  
555 warm-rain microphysics and aqueous chemistry. *Journal of Open Source Soft-*  
556 *ware*, *7*(72), 3219. doi: 10.21105/joss.03219
- 557 Berry, E. X. (1967). Cloud Droplet Growth by Collection. *Journal of Atmospheric*  
558 *Sciences*, *24*(6), 688–701. doi: 10.1175/1520-0469(1967)024(0688:CDGBC)2.0  
559 .CO;2
- 560 Berry, E. X., & Reinhardt, R. L. (1974). An Analysis of Cloud Drop Growth by  
561 Collection: Part I. Double Distributions. *Journal of the Atmospheric Sciences*,  
562 *31*(7), 1814–1824. doi: 10.1175/1520-0469(1974)031(1814:AAOCDG)2.0.CO;2
- 563 Bieli, M., Dunbar, O., de Jong, E. K., Jaruga, A., Schneider, T., & Bischoff, T.  
564 (n.d.). *An efficient Bayesian approach to learning droplet collision kernels:*  
565 *Proof of concept using "Cloudy", a new n-moment bulk microphysics scheme.*  
566 doi: 10.1002/essoar.10510248.1
- 567 Bott, A. (1998). A Flux Method for the Numerical Solution of the Stochastic Collec-  
568 tion Equation. *Journal of the Atmospheric Sciences*, *55*(13), 2284–2293. doi:  
569 10.1175/1520-0469(1998)055(2284:AFMFTN)2.0.CO;2
- 570 Filbet, F., & Laurençot, P. (2004). Numerical Simulation of the Smoluchowski Co-  
571 agulation Equation. *SIAM Journal on Scientific Computing*, *25*(6), 2004–2028.  
572 doi: 10.1137/S1064827503429132
- 573 Franke, C., & Schaback, R. (1998). Solving partial differential equations by col-  
574 location using radial basis functions. *Applied Mathematics and Computation*,  
575 *93*(1), 73–82. doi: 10.1016/S0096-3003(97)10104-7
- 576 Gelbard, F., & Seinfeld, J. H. (1978). Numerical solution of the dynamic equation  
577 for particulate systems. *Journal of Computational Physics*, *28*(3), 357–375.  
578 doi: 10.1016/0021-9991(78)90058-X
- 579 Gettelman, A., Gagne, D. J., Chen, C.-C., Christensen, M. W., Lebo, Z. J., Mor-  
580 rison, H., & Gantos, G. (2021). Machine Learning the Warm Rain Process.  
581 *Journal of Advances in Modeling Earth Systems*, *13*(2), e2020MS002268. doi:  
582 10.1029/2020MS002268
- 583 Ghan, S. J., Abdul-Razzak, H., Nenes, A., Ming, Y., Liu, X., Ovchinnikov, M., ...  
584 Shi, X. (2011). Droplet nucleation: Physically-based parameterizations and  
585 comparative evaluation. *Journal of Advances in Modeling Earth Systems*, *3*(4).  
586 doi: 10.1029/2011MS000074
- 587 Golovin, A. M. (1963). The Solution of the Coagulation Equation for Raindrops.  
588 Taking Condensation into Account. *Izv. Akad. Nauk. SSSR. Ser. Geofiz.*, *5*,  
589 783–791.
- 590 Intergovernmental Panel on Climate Change. (2014). *Climate Change 2013 – The*  
591 *Physical Science Basis: Working Group I Contribution to the Fifth Assess-*

- 592 *ment Report of the Intergovernmental Panel on Climate Change.* Cambridge:  
593 Cambridge University Press. (doi: 10.1017/CBO9781107415324)
- 594 Kessler, E. (1969). On the Distribution and Continuity of Water Substance in At-  
595 mospheric Circulations. In E. Kessler (Ed.), *On the Distribution and Continu-*  
596 *ity of Water Substance in Atmospheric Circulations* (pp. 1–84). Boston, MA:  
597 American Meteorological Society. (doi: 10.1007/978-1-935704-36-2\_1)
- 598 Khain, A. P., Beheng, K. D., Heymsfield, A., Korolev, A., Krichak, S. O., Levin, Z.,  
599 ... Yano, J.-I. (2015). Representation of microphysical processes in cloud-  
600 resolving models: Spectral (bin) microphysics versus bulk parameterization.  
601 *Reviews of Geophysics*, 53(2), 247–322. doi: 10.1002/2014RG000468
- 602 Lebo, Z. J., & Seinfeld, J. H. (2011). A continuous spectral aerosol-droplet micro-  
603 physics model. *Atmospheric Chemistry and Physics*, 11(23), 12297–12316. doi:  
604 10.5194/acp-11-12297-2011
- 605 Milbrandt, J. A., & Yau, M. K. (2005). A Multimoment Bulk Microphysics Parame-  
606 terization. Part I: Analysis of the Role of the Spectral Shape Parameter. *Jour-*  
607 *nal of the Atmospheric Sciences*, 62(9), 3051–3064. doi: 10.1175/JAS3534.1
- 608 Morrison, H., & Grabowski, W. W. (2007). Comparison of Bulk and Bin Warm-  
609 Rain Microphysics Models Using a Kinematic Framework. *Journal of the At-*  
610 *mospheric Sciences*, 64(8), 2839–2861. doi: 10.1175/JAS3980
- 611 Morrison, H., & Grabowski, W. W. (2008). Modeling Supersaturation and Subgrid-  
612 Scale Mixing with Two-Moment Bulk Warm Microphysics. *Journal of Atmo-*  
613 *spheric Sciences*, 65(3), 792–812. doi: 10.1175/2007JAS2374.1
- 614 Morrison, H., Lier-Walqui, M. v., Fridlind, A. M., Grabowski, W. W., Harrington,  
615 J. Y., Hoose, C., ... Xue, L. (2020). Confronting the Challenge of Modeling  
616 Cloud and Precipitation Microphysics. *Journal of Advances in Modeling Earth*  
617 *Systems*, 12(8). doi: 10.1029/2019MS001689
- 618 Morrison, H., & Milbrandt, J. A. (2015). Parameterization of Cloud Microphysics  
619 Based on the Prediction of Bulk Ice Particle Properties. Part I: Scheme De-  
620 scription and Idealized Tests. *Journal of the Atmospheric Sciences*, 72(1),  
621 287–311. doi: 10.1175/JAS-D-14-0065.1
- 622 Morrison, H., van Lier-Walqui, M., Kumjian, M. R., & Prat, O. P. (2019). A  
623 Bayesian Approach for Statistical–Physical Bulk Parameterization of Rain Mi-  
624 crophysics. Part I: Scheme Description. *Journal of the Atmospheric Sciences*,  
625 77(3), 1019–1041. doi: 10.1175/JAS-D-19-0070.1
- 626 Rackauckas, C., & Nie, Q. (2017). DifferentialEquations.jl – A Performant and  
627 Feature-Rich Ecosystem for Solving Differential Equations in Julia. *Journal of*  
628 *Open Research Software*, 5(1), 15. doi: 10.5334/jors.151
- 629 Randall, D., Khairoutdinov, M., Arakawa, A., & Grabowski, W. (2003). Breaking  
630 the Cloud Parameterization Deadlock. *Bulletin of the American Meteorological*  
631 *Society*, 84(11), 1547–1564. doi: 10.1175/BAMS-84-11-1547
- 632 Riechermann, T., Noh, Y., & Raasch, S. (2012). A new method for large-eddy  
633 simulations of clouds with Lagrangian droplets including the effects of turbu-  
634 lent collision. *New Journal of Physics*, 14(6). doi: 10.1088/1367-2630/14/6/  
635 065008
- 636 Rodríguez Genó, C. F., & Alfonso, L. (2022). Parameterization of the colli-  
637 sion–coalescence process using series of basis functions: COLNETv1.0.0 model  
638 development using a machine learning approach. *Geoscientific Model Develop-*  
639 *ment*, 15(2), 493–507. doi: 10.5194/gmd-15-493-2022
- 640 Seifert, A., & Beheng, K. D. (2006). A two-moment cloud microphysics parameter-  
641 ization for mixed-phase clouds. Part 1: Model description. *Meteorology and At-*  
642 *mospheric Physics*, 92(1-2), 45–66. doi: 10.1007/s00703-005-0112-4
- 643 Shima, S., Kusano, K., Kawano, A., Sugiyama, T., & Kawahara, S. (2009). The  
644 super-droplet method for the numerical simulation of clouds and precipita-  
645 tion: a particle-based and probabilistic microphysics model coupled with a  
646 non-hydrostatic model. *Quarterly Journal of the Royal Meteorological Society*,

647 135(642), 1307–1320. doi: 10.1002/qj.441  
 648 Stephens, G. L., L’Ecuyer, T., Forbes, R., Gettelmen, A., Golaz, J.-C., Bodas-  
 649 Salcedo, A., . . . Haynes, J. (2010). Dreary state of precipitation in global  
 650 models. *Journal of Geophysical Research: Atmospheres*, 115(24). doi:  
 651 10.1029/2010JD014532  
 652 Tzivion (Tzitzvashvili), S., Feingold, G., & Levin, Z. (1987). An Efficient Numerical  
 653 Solution to the Stochastic Collection Equation. *Journal of Atmospheric Sci-*  
 654 *ences*, 44(21), 3139–3149. doi: 10.1175/1520-0469(1987)044<3139:AENSTT>2.0  
 655 .CO;2  
 656 Wu, Z. (1995). Compactly supported positive definite radial functions. *Advances in*  
 657 *Computational Mathematics*, 4(1). doi: 10.1007/BF03177517  
 658 Young, K. C. (1974). A Numerical Simulation of Wintertime, Orographic Pre-  
 659 cipitation: Part I. Description of Model Microphysics and Numerical Tech-  
 660 niques. *Journal of the Atmospheric Sciences*, 31(7), 1735–1748. doi:  
 661 10.1175/1520-0469(1974)031<1735:ANSOWO>2.0.CO;2  
 662 Zhang, X., Song, K. Z., Lu, M. W., & Liu, X. (2000). Meshless methods based on  
 663 collocation with radial basis functions. *Computational Mechanics*, 26(4), 333–  
 664 343. doi: 10.1007/s004660000181